Research Article Vol. 13, No. 3 / 1 Mar 2022 / Biomedical Optics Express 1261
Biomedical Optics EXPRESS

Quantitative measurement of optical properties and Hb concentration in a rodent model of inflammatory Meibomian gland dysfunction using spatial frequency domain imaging

HYEONGBEOM KIM,[1] KYONG JIN CHO,[2] ANTHONY J. DURKIN,[3] BRUCE J. TROMBERG,[4] AND ILYONG PARK[1,5,*]

[1]Department of Biomedical Engineering, College of Medicine, Dankook University, Cheonan, Republic of Korea
[2]Department of Ophthalmology, College of Medicine, Dankook University, Cheonan, Republic of Korea
[3]Beckman Laser Institute and Medical Clinic, University of California, Irvine, USA
[4]National Institute of Biomedical Imaging and Bioengineering, National Institutes of Health, Bethesda, Maryland, USA
[5]Beckman Laser Institute Korea, College of Medicine, Dankook University, Cheonan, Republic of Korea
*piyong@dankook.ac.kr

Abstract: Herein, to investigate a new diagnostic method for Meibomian gland dysfunction (MGD) induced by eyelid inflammation, optical properties and deoxy-hemoglobin (Hb) concentrations in rodent eyelid tissues, including Meibomian glands(MGs), were measured using spatial frequency domain imaging (SFDI). Complete Freund's adjuvant solutions were injected into the eyelid margins of Sprague–Dawley rats to induce MGD. After three weeks, the optical properties and Hb of the MG and non-MG regions of the eyelids were measured *ex–vivo* using an SFDI system. The comparison of Hb showed that the MGD group exhibited significantly higher values than those of the control group in both regions. The optical properties at 730 and 850 nm for the MG regions in the MGD group were significantly different from those in the control group. In addition, the 630 nm absorption coefficients of both regions were significantly higher in the MGD group than in the control group. Thus, the SFDI technique can detect the increased Hb concentration and changes in the optical properties of the eyelids due to inflammatory MGD in a noncontact manner and has the potential to be used as a novel quantitative diagnostic method for the occurrence of MGD.

1. Introduction

Meibomian gland (MG) is a sebaceous gland located inside the upper and lower tarsal plates of the eyelids [1]. The MG secretes lipid-containing substances in the outermost part of the tear film, preventing the evaporation of tears and acting as a lubricant between the eye surface and eyelids in blink movements [2]. However, when Meibomian gland dysfunction (MGD) occurs and the secretion of MG is abnormally reduced, the evaporation of tears is accelerated, which can cause evaporative dry eye [3,4]. A major cause of MGD is eyelid inflammation and swelling. As shown in Fig. 1, when inflammation occurs in the eyelids, the blood flow increases by the extension of blood vessels in the tissue. In addition, swelling occurs by the escape of plasma from the vessel to the tissue [5]. The inflammation changes the quantity and quality of the meibum, resulting in tear film instability [6]. Through this process, the MG enters the inflammatory MGD stage. In addition, the lipid concentration in the MG is increased. If the inflammatory MGD persists, it can develop into a chronic MGD, which leads to the extinction of MGs. Detection of MGD triggers due to eyelid tissue inflammation is useful for an early diagnosis and treatment of the MGD.

#449150 https://doi.org/10.1364/BOE.449150
Journal © 2022 Received 22 Nov 2021; revised 13 Jan 2022; accepted 19 Jan 2022; published 4 Feb 2022

Biomedical Optics EXPRESS

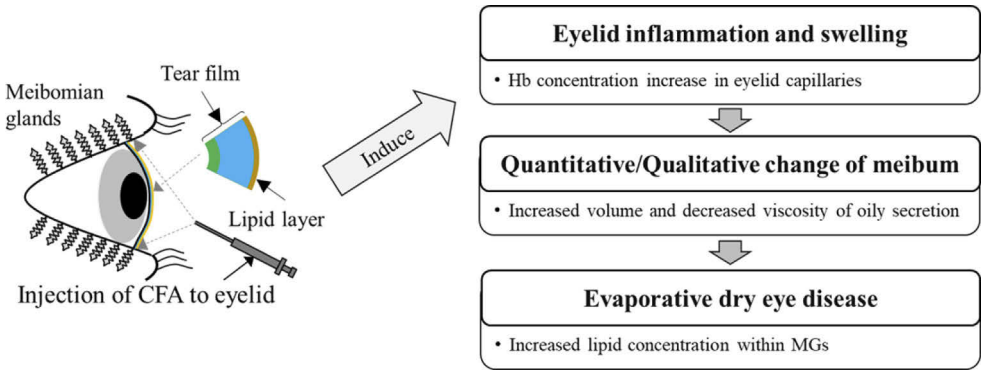

Fig. 1. Vicious cycle of inflammatory MGD induced by complete Freund's adjuvant (CFA) injection.

Conventional methods for diagnosis of MGD include morphological structural inspection using meibography [7–10] and lipid component level measurement using meibometry [11,12]. Meibography is a method used to acquire a structural image of the MG by projecting near-infrared (NIR) light to the MG with an IR camera. Meibography enables diagnosis of evaporative dry eye syndrome by assessing the loss of MGs. Meibometry is a method for diagnosing MGD by measuring the level of lipid components secreted by the MG by attaching a translucent plastic tape to the eyelids for 10 s and allowing it to accumulate secreted lipid. In addition, the tear film break-up time (T-BUT) [13] may be used as an indirect assessment measure without directly measuring the MG. T-BUT measures the time required for the tear film to break. Black spots appear on the ocular surface using fluorescein staining. If the tear film breaks faster than the normal range, dry eye syndrome is diagnosed. T-BUT is mostly affected by the amount and quality of the tear film layers. As the decrease in MG secretion affects the lipid layer in the tear film leading to a shorter T-BUT, the measurement of MG secretion can also be used as a diagnostic indicator of MGD [13–15]. As mentioned above, the existing methods do not directly provide quantitative information about eyelid tissues with MGs that are affected by inflammatory MGD, as they are based on morphological structural examination of MGs or measurement of the secreted components. In this regard, a novel measurement technique capable of noncontact investigation of whether or not the eyelid tissue containing MG corresponds to the stage of inflammatory MGD can be used for an early diagnosis of MGD.

Spatial frequency domain imaging (SFDI) [16–23] is an optical imaging technique that can effectively separate and quantify the absorption and reduced scattering coefficient of turbid media such as human tissues using reflectance measured with spatial frequency modulated light sources. The technique is a noninvasive, noncontact, and quantitative imaging method. In addition, tissue chromophore concentrations can be deduced from the absorption coefficients at different wavelengths. Because of these features of SFDI, we employed the SFDI method to investigate the difference in components and optical properties of the inflamed eyelid tissues that cause MGD compared to normal eyelid tissues. The optical properties and deoxy-hemoglobin (Hb) concentrations of the MG tissue and eyelid tissue around the MG obtained through SFDI were compared between MGD and control groups. Some image segmentation processing methods have been used to isolate MG regions from eyelid images obtained using SFDI. Through this study, it was evaluated whether quantitative differences in the MGs and eyelid tissues with inflammatory MGD could be observed with SFDI.

Biomedical Optics EXPRESS

2. Methods

2.1. SFDI instrumentation

We designed the SFDI system shown in Fig. 2 to measure *ex-vivo* eyelid tissues and MGs of rats. The light source was a digital micromirror device chip-based light-emitting diode (LED) projector (P450, AAXA Technologies, Irvine, CA, USA). For optical property measurements of the *ex-vivo* tissue and MG, the blue and green-LEDs inside the projector were replaced with 730- and 850-nm NIR LEDs. In addition, the internal visible-wavelength beam combiners were replaced with 685 and 801 nm long-pass dichroic mirrors (FF801, FF685, Semrock, Rochester, NY, US). The camera used for image acquisition was a monochrome charge-coupled device camera (CM3-U3-13S2M-CS, FLIR, Wilsonville, OR, US) with a focusing lens (M7528-MP, Computar, Cary, NC, US). In addition, optical bandpass filters (FB630, FB730, and FB830, Thorlabs, Newton, NJ, US) mounted on a filter wheel were placed between the camera and sample to pass the desired wavelength light. Each polarizer (LPNIRE-B, Thorlabs, Newton, NJ, US) was placed in front of the projector and camera to remove specular reflection light from the surface. We used a sample plate consisting of a white PVC foam sheet and an adjustable height support jack to keep the distance between the sample and the camera constant. The system control and analysis programs were implemented using MATLAB (The MathWorks, Natick, MA, US). The actual implementation is shown in Fig. 3. The field of view of the implemented system was 23 mm × 12 mm, while the measured image resolution was 1288 × 964 pixels.

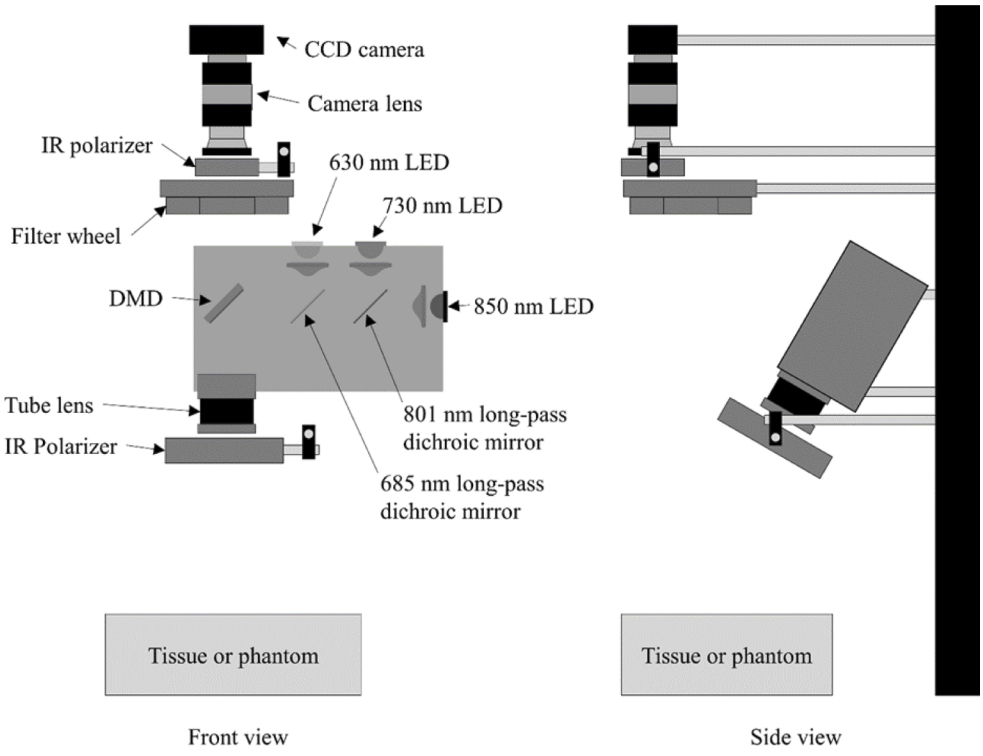

Fig. 2. Schematic of the SFDI system designed for *ex-vivo* eyelid tissue measurements in rats.

Biomedical Optics EXPRESS

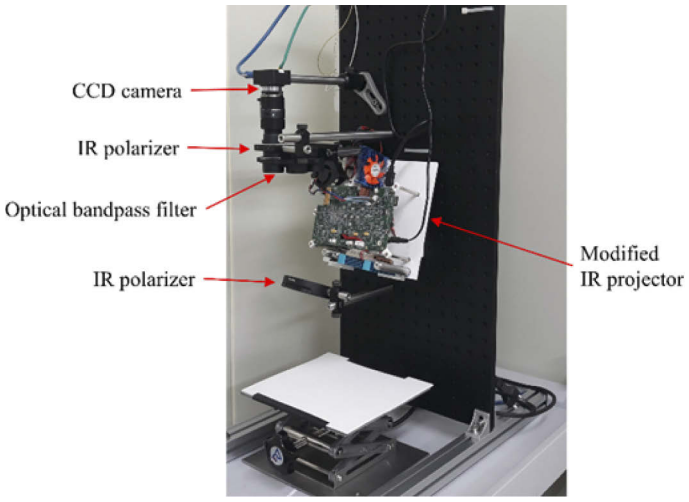

Fig. 3. Implemented SFDI system for an *ex-vivo* eyelid tissue measurement.

2.2 MGD rat models

The animals used in this study were 6-week-old female Sprague–Dawley (SD) rats. Four rats per group were used for the experiment. MGD was induced in rats based on the method of Miyake et al. [24]. First, using local anesthesia, 10 μL of complete Freund's adjuvant (CFA) was injected into the nasal, central, and temporal regions of the upper and lower eyelid margins to induce eyelid inflammation, as shown in Fig. 1. Subsequently, the rats were housed for 22 days in cages with 12–12-h light/dark cycles. The temperature and humidity were maintained at 24 ± 1 °C and 55 ± 10%, respectively. After 22 days, we carried out the T-BUT test [13] and lid margin swelling score (0 = absent, 1 = mild, 2 = moderate, and 3 = severe) measurement [25] on the rats to verify the MGD induction. Since these *in-vivo* tests were performed on the left and right eyes, respectively, the intended number of eyes tested in each group is 8. However, one of the eyes in the control group was excluded from the study because it was non-diagnosable state due to eye damage. Thereafter, the rats were sacrificed and the eyelids with MGs were excised. During the excision process, many eyelids were contaminated by blood and hair. Even if the contaminated eyelid was thoroughly washed, it was impossible to use the eyelids for the *ex-vivo* measurement due to bloodstains and MG damage. So, five clean eyelids with intact MGs in each group were selected for SFDI imaging. The thickness of a sampled eyelid is about 2.7 mm. The width and length of the eyelid and MG array are roughly 10 mm × 20 mm and 1 mm × 7 mm. An MG array consists of multiple MGs (~15 MGs). A single MG has the width and length of about 0.3mm × 1 mm. The spacing distance between two adjacent MGs is about 0.1 mm. All experiments were approved by the Dankook University Institutional Animal Care & Use Committee and performed in compliance with the regulations (approval no. DKU-19-002).

2.2. Image acquisition and analysis

To measure optical properties and Hb in the eyelids of rats, we acquired images of the eyelid tissues with MGs using three wavelengths (630, 730, and 850 nm) and two spatial frequencies (0 and 0.2 mm^{-1}). In addition, eyelid images corresponding to three phases (0°, 120°, and 240°) were obtained for each spatial frequency for the demodulation of the spatial-frequency-modulated image. In summary, 18 images were acquired for each eyelid tissue sample. The acquired image was analyzed using a reported SFDI analysis method [16–19]. Figure 4 summarizes the entire analysis process.

Biomedical Optics EXPRESS

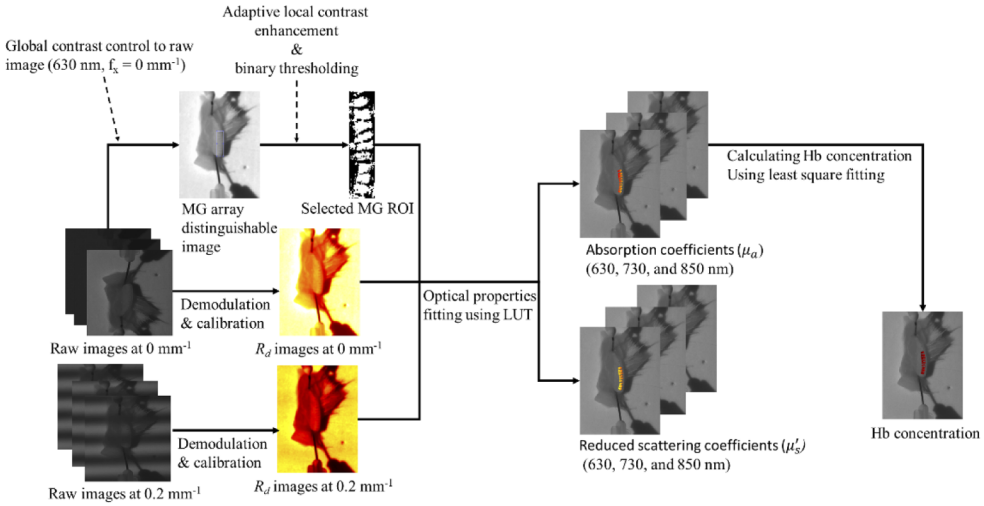

Fig. 4. Analysis flow chart of the measured *ex-vivo* eyelid tissue images. Solid lines indicate the sequence and flow of analysis. The dashed line indicates the analysis technique that follows the solid line. Based on the process shown in the figure, the values of the absorption and reduced scattering coefficients for each wavelength and Hb concentration are obtained. The LUT refers to the two-spatial-frequency LUT.

The obtained raw images were spatial-frequency-modulated reflectance images. Each raw image was demodulated to obtain the alternating-current (AC) brightness component (M_{AC}) and direct-current (DC) brightness component (M_{DC}). For the demodulation of the raw images, we used a method using three-phase images with the same spatial frequency in the experiment to reduce the influence of light brightness and minimize the frequency component loss [17,26]. Demodulation can be achieved by

$$M_{AC}(x_i) = \frac{\sqrt{2}}{3}\sqrt{\{[I_1(x_i) - I_2(x_i)]^2 + [I_2(x_i) - I_3(x_i)]^2 + [I_3(x_i) - I_1(x_i)]^2\}}, \quad (1)$$

$$M_{DC}(x_i) = \frac{1}{3}[I_1(x_i) + I_2(x_i) + I_3(x_i)], \quad (2)$$

where $I_p(x_i)$ denotes the light intensity at the pixel of the i^{th} index and p^{th} phase at 0°, 120°, and 240°. M_{AC} obtained through this demodulation contains diffuse reflectance information that removes the effects of ambient light brightness and optical system's characteristics. To eliminate the effect of light brightness and characteristics of the optical system, a reference phantom with known reflectance and optical properties was measured using our SFDI and calibrated [17]. The calibration was performed by

$$R_d = \frac{M_{AC}(x_i)}{M_{AC.ref}(x_i)} \cdot R_{d.ref}. \quad (3)$$

The reference phantom reflectance ($R_{d.ref}$) and its optical properties were measured using a reference SFDI system (Spatial Frequency Domain Spectroscopy system [27], Beckman Laser Institute, UC Irvine). The AC brightness component of the reference phantom ($M_{AC.ref}$) can be used to calibrate the sample tissue M_{AC} to obtain the tissue reflectance (R_d). R_d for the spatial frequencies of 0 and 0.2 mm^{-1} obtained through this procedure were used to fit the optical properties by the two-spatial-frequency look-up table (LUT) methods [18].

It is possible to separate the optical properties of the absorption coefficient and reduced scattering coefficient using this process. Moreover, the chromophore concentrations can be

Biomedical Optics EXPRESS

obtained from the linear combination of the measured absorption coefficients and known extinction coefficients at multiple wavelengths using an equation solver. We obtained the Hb concentrations by applying a constrained linear least-squares fitting technique to determine the chromophore concentration change of the eyelid tissue due to inflammation. As the eyelids were measured after 30 min to 1 h from the time of excision, we assumed that all oxygen was almost depleted and oxy-hemoglobin (HbO_2) was excluded from the chromophore measurement.

We aimed to compare the Hb concentrations and reduced scattering coefficients for each group obtained by the measurement. However, as the shape of the MGs was a curved comb in the acquired image, it was expected that the comparison of average values through a simple rectangular region of interest (ROI) was not appropriate. To compare only intact MGs, we applied adaptive local contrast enhancement [28] and binary thresholding techniques to compare the mean values by selecting only the MG parts, as shown in Fig. 5. The optical properties of the eyelid in the non-MG regions (the red box in Fig. 7(a) shows this region) were compared to the MG part values. Two-way ANOVA test and Bonferroni post hoc test were performed using Prism5 (GraphPad, San Diego, CA, US) for each parameter to identify significant differences between the MGD and control groups. All analytical processes were carried out in MATLAB R2015a (MathWorks, Natick, MA, US).

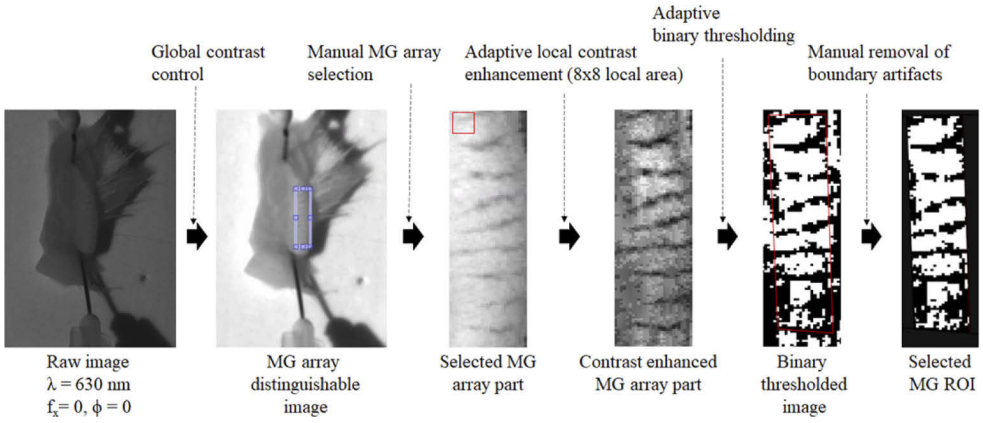

Fig. 5. Image processing for selecting an MG ROI within an MG array as possible as the ROI represents the MG morphology.

3. Results

3.1. Verification of MGD induction using the T-BUT test and MG swelling measurement

The results of the conventional method are presented in Fig. 6. The mean value of the T-BUTs measured in the MGD group (N = 8) was approximately 2.467 s. The MGD group's T-BUT was shorter than approximately 7.976 s in the control group (N = 7) (Fig. 6(a)). The meibum emissions of the MGD group were affected by the CFA injection. In addition, the mean value of the lid margin swelling score in the MGD group (N = 8) was approximately 2 (moderate), which was higher than that of the control group (N = 7) (Fig. 6(b)). We confirmed that MGD caused by meibomitis was successfully induced in the MGD group.

3.2. Comparison of absorption coefficient maps

The measured absorption coefficient maps of the MG region are shown in Fig. 7(a). The graphs in Fig. 7(b) indicate the mean values of the absorption coefficients for each group. In the MG region, the mean absorption coefficients of the MGD group ($N = 5$) were 0.027, 0.013, and 0.010

Biomedical Optics EXPRESS

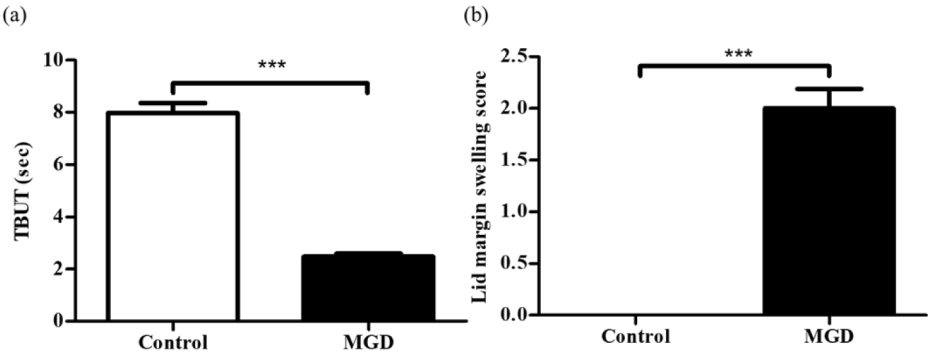

Fig. 6. Comparison of conventional MG diagnosis method results. (a) T-BUT test results. (b) Measured lid margin swelling results (***: $p < 0.001$). All results are shown as mean ± standard error.

mm^{-1} at 630, 730, and 850 nm, respectively. These values were higher than the mean values in the control group, which were 0.012, 0.006, and 0.004 mm^{-1}, respectively. These values were significantly different ($p < 0.01$) at all wavelengths between the MGD and control groups. Similarly, the mean absorption coefficients of the non-MG areas in the MGD group (0.020, 0.006, and 0.005 mm^{-1}) were higher than those of the control group (0.009, 0.004, and 0.003 mm^{-1}, respectively). The absorption coefficient increase in the eyelid region in the MGD group indicates a change in chromophore concentration, such as an increase in Hb concentration caused by eyelid inflammation and MGD. In addition, the 730-nm and 850-nm absorption coefficients of MG regions in the MGD group were significantly different from those in the non-MG regions of the same group ($p < 0.01$). Because the MG region has a lipid component unlike the non-MG region eyelid, the disparate chromophore components in the two regions appear as the differences in the absorption coefficients.

3.3. Comparison of Hb concentrations

The Hb concentration map of the MGs measured using SFDI is shown in Fig. 8(a). The mean Hb concentration of the MG regions in the MGD group was 52.229 μM, which was considerably higher than the value of 25.145 μM for the MG regions in the control group ($p < 0.01$), as shown in Fig. 8(b). In addition, the mean Hb concentration of the non-MG regions measured in the MGD group was 38.214 μM, which was higher than the value of 17.907 μM for the non-MG regions in the control group ($p < 0.05$). The increased Hb concentration in the MGD group results from the blood flow increase with dilated blood vessels caused by inflammation.

3.4. Comparison of reduced scattering coefficient maps

The reduced scattering coefficient map of the MG measured using the SFDI is shown in Fig. 9(a). As shown in Fig. 9(b), the mean reduced scattering coefficients of the MG regions in the MGD group ($N = 5$) were 1.641, 1.451, and 1.404 mm^{-1} at 630, 730, and 850 nm, respectively, whereas those of the MG regions in the control group ($N = 5$) were 1.891, 1.771, and 1.733 mm^{-1}, respectively. Furthermore, the MG regions' reduced scattering coefficients at the wavelengths of 730 and 850 nm, except at 630 nm, exhibited significant differences between the two groups ($p < 0.05$). The mean reduced scattering coefficients of the non-MG regions in the MGD group were 1.002, 0.927, and 0.848 mm^{-1} at 630, 730, and 850 nm, respectively, whereas those of non-MG regions in the control group ($N = 5$) were 1.683, 1.633, and 1.690 mm^{-1}, respectively. There were significant differences ($p < 0.001$) at all wavelengths between the MGD and control groups, as for the results of MG regions. The reason for the decrease in the reduced scattering

Biomedical Optics EXPRESS

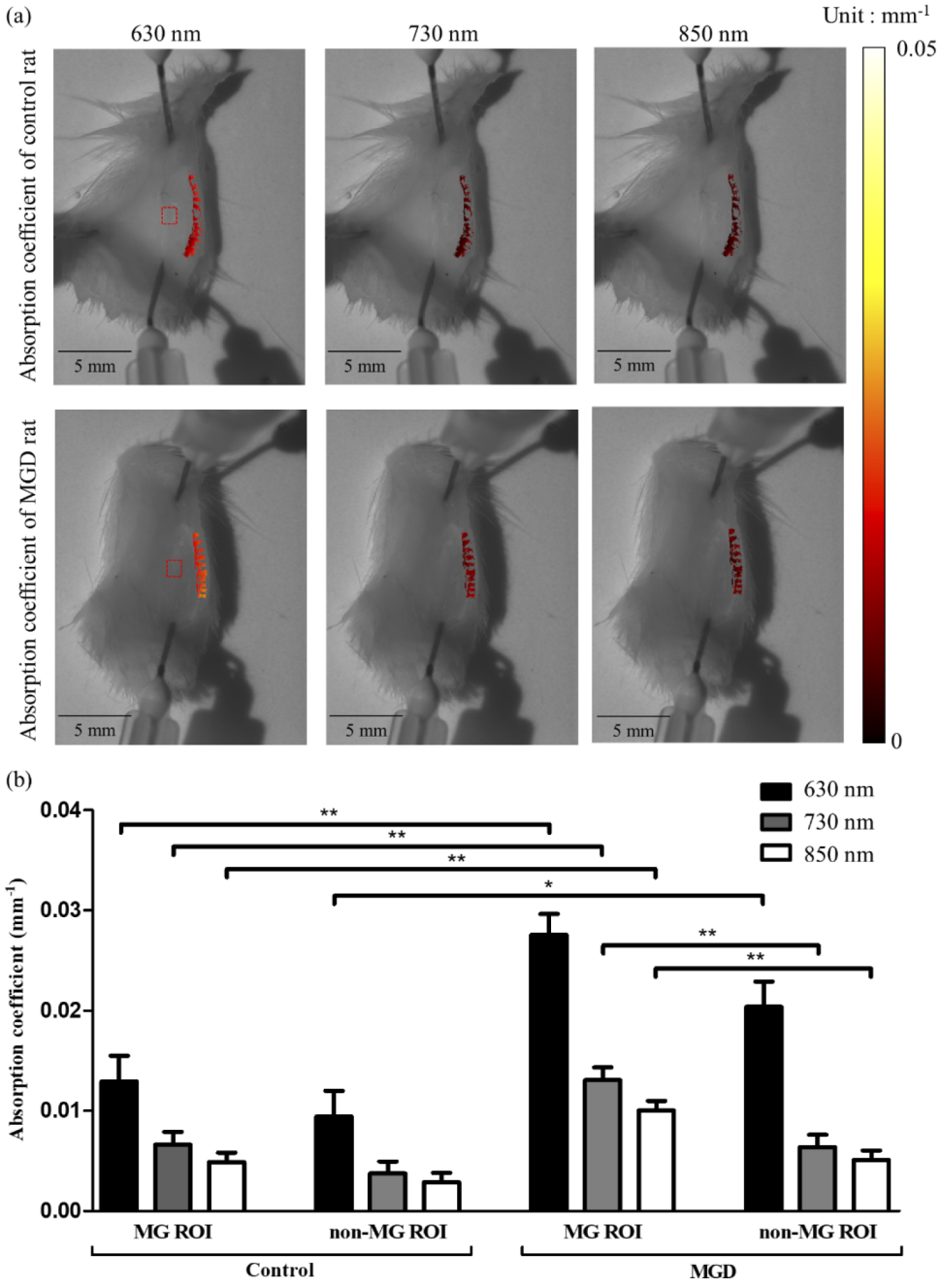

Fig. 7. Absorption coefficient comparison of the MG at a ROI between the MGD and control groups. (a) Measured absorption coefficient maps of both groups. The dashed red box shows the eyelid of non-MG regions. (b) Comparison of the measured absorption coefficients of the control and MGD groups. The results of (b) are shown as mean ± standard error (*: $p < 0.05$, **: $p < 0.01$).

Biomedical Optics EXPRESS

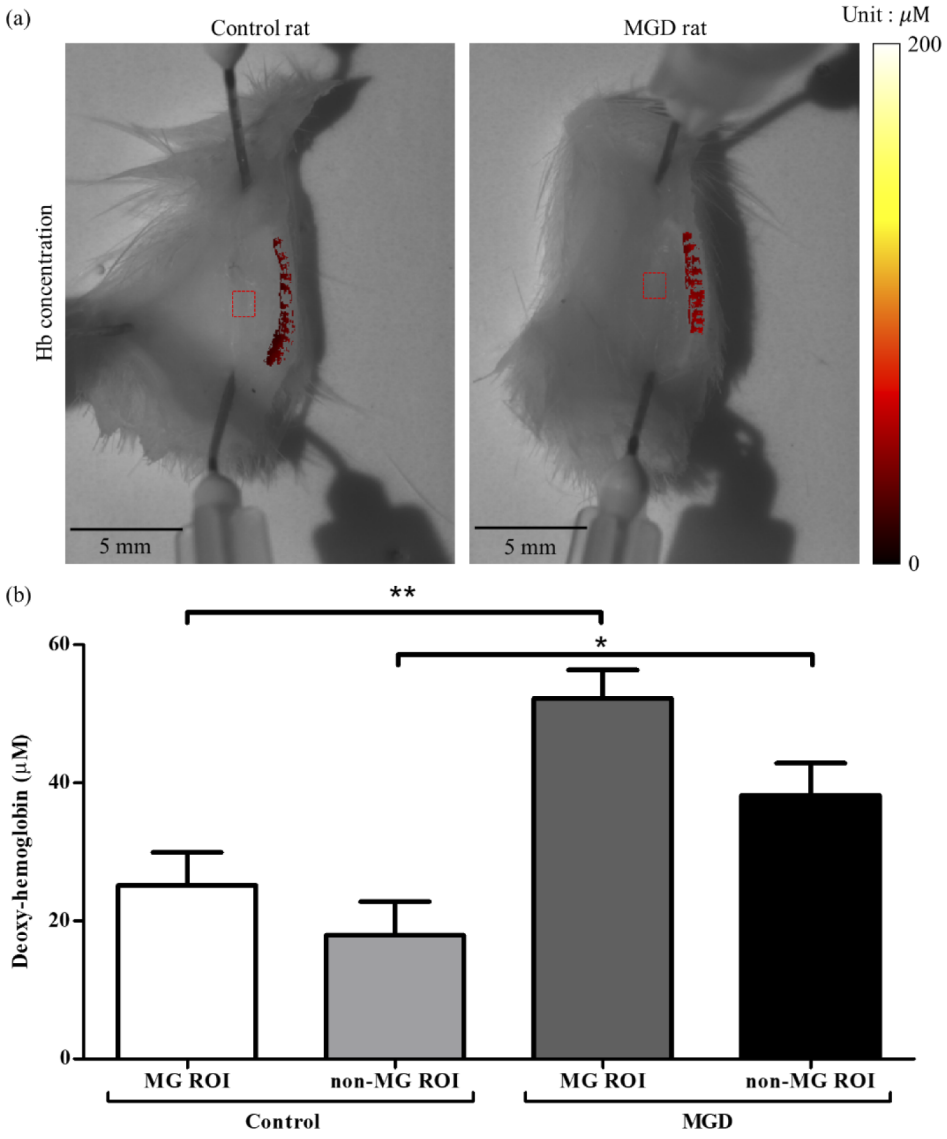

Fig. 8. Comparison of deoxy-hemoglobin (Hb) results. (a) Measured Hb concentration maps of the control and MGD groups. (b) Comparison of the Hb concentrations of the control and MGD groups. The results of (b) are shown as mean ± standard error (*: $p < 0.05$, **: $p < 0.01$). The dashed red box shows the eyelid of non-MG regions.

Biomedical Optics EXPRESS

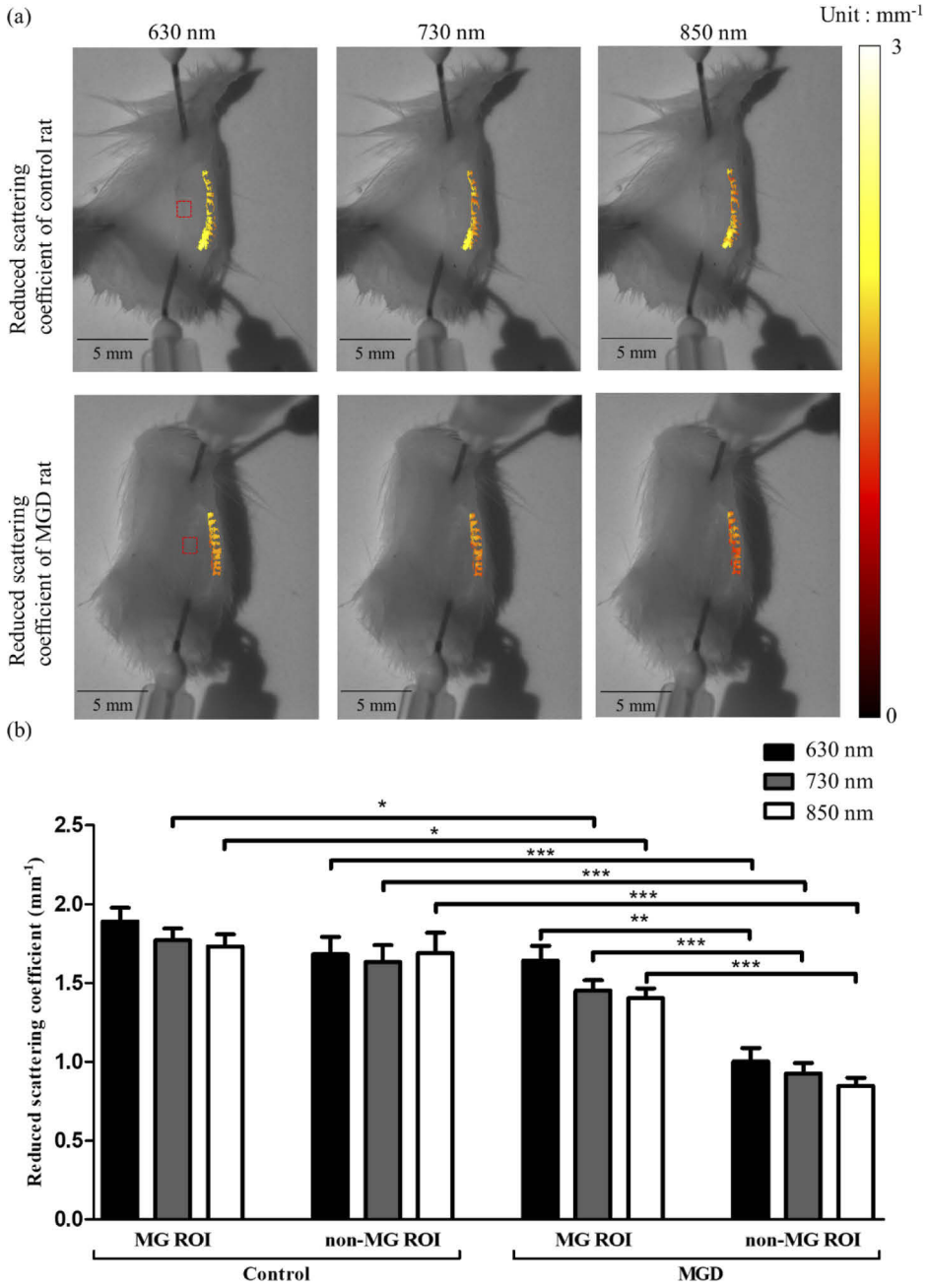

Fig. 9. Reduced scattering coefficient comparison of the MG at a ROI between the MGD and control groups. (a) Measured reduced scattering coefficient maps of both groups. The dashed red box shows the eyelid of non-MG regions. (b) Comparison of the measured reduced scattering coefficients of the control and MGD groups. The results of (b) are shown as mean ± standard error (*: $p < 0.05$, **: $p < 0.01$,***: $p < 0.001$).

Biomedical Optics EXPRESS

coefficient is probably the volume expansion and scatterer decrease per unit volume of the inner tissue by swelling due to inflammation. In addition, the reduced scattering coefficients of the MG regions in the MGD group were significantly higher than those in the non-MG regions of the same group, because the concentration of lipids that have strong scattering properties is increased in the MG regions. In the control group, the reduced scattering coefficient of the MG region was not significantly different from the non-MG region. Normal MG produces lipids and secrets them through MG orifices without lipid stagnant and accumulation. So, in case the control group, the lipid concentration of MG region is not so large enough that the reduced scattering coefficients between MG and non-MG region shows significant difference.

4. Discussion

When CFA is applied to the eyelids, inflammation usually develops, along with changes in meibum quantity and quality [24]. Changes in meibum cause early-stage MGD, tear firm instability, and lipid concentration increase in the MG area. We performed T-BUT and swelling score tests to evaluate the inflammation and MGD in CFA-injected SD rats. In this study, the T-BUT of MGD-induced SD rats was significantly shorter than that of the control-group T-BUT. Swelling occurred in the eyelids of MGD-induced SD rats. These results verified that the early-stage MGD and inflammation were induced in the MG of MGD-group SD rats. If this early stage of MGD persists, bacteria multiply in the meibum and the inflammation and MGD intensify, leading to chronic evaporative dry eye disease. In this study, we used SFDI to evaluate the early stage of MGD by measuring the optical properties and Hb concentration changes before intensifying to chronic dry eye disease.

As shown in Fig. 7, in the non-MG regions, only the absorption coefficient at 630 nm was significantly different between the MGD and control groups. As Hb has a higher absorption at 630 nm than at 730 and 850 nm, the increase rate of the 630-nm absorption coefficient in the non-MG regions according to the Hb concentration increase due to the eyelid tissue inflammation might be higher than those of the 730- and 850-nm absorption coefficients. However, for the MG regions, significant differences were observed at all wavelengths between the two groups. As the lipid absorbs the 730- and 850-nm light more than that at 630 nm, all absorption coefficients of the MG regions where the inflammatory MGD increased the lipid concentration within MGs might exhibit significant differences between the two groups. Likewise, in the MGD group results, the increased lipid concentration of the MG regions might lead to 730- and 850-nm absorption coefficients of the MG regions significantly higher than those of the non-MG regions (p value at 730 nm = 0.0159, p value at 850 nm = 0.0079). In the case of the 630-nm absorption coefficient, the measured value in the MG area was higher than that in the non-MG, but there was no significant difference (p value at 630 nm = 0.0952). In this regard, the measured absorption coefficients may be affected by swelling and increased lipid concentration due to inflammatory MGD. To further demonstrate the correlation between the measured absorption coefficients and lipid concentrations of the MGD eyelid tissues, we need to further investigate the quantitative measurement of lipid concentrations using shortwave IR (SWIR) SFDI.

An inflamed eyelid increases Hb and HbO_2 concentrations due to an increase in blood vessels and blood flow. The concentration change affects the absorption coefficient of eyelid tissues, including MGs. In the MG region results, the absorption coefficients of the MGD group measured by the implemented SFDI system were significantly higher than those of the control system. The measured Hb concentrations in the MGD group were also significantly higher than those in the control group. These results demonstrate that the eyelid tissue component change due to inflammatory MGD could be detected by the SFDI method, which measures the optical properties and Hb concentration of the eyelids. In this experiment, we did not consider the HbO_2 chromophore when the SFDI method was used, because the obtained eyelid sections were assumed to be oxygen-depleted after tissue extraction and the eyelids could not receive oxygen

Biomedical Optics EXPRESS

via blood vessels. So, we considered three chromophores existing in the eyelids such as Hb, water, and lipid. Though we could obtain Hb concentration, water, and lipid fraction through the SFDI measurement, we focused only on Hb concentration as a meaningful chromophore because Hb plays a major light absorber in the eyelid tissue unlike water and lipid which has very low absorption in the wavelengths of 630, 730, and 850 nm. In case of severely damaged tissues like burn tissues, it is recommended to consider methemoglobin in the chromophore concentration calculation for accurate Hb concentration measurement [29]. Unlike the severely damaged tissue, however, the excised eyelid tissues in our experiment may produce slowly the methemoglobin by the small tissue injury. And we think the amount of accumulated methemoglobin in eyelid tissues was not considerable because we finished all SFDI measurements within 2 hours after excising eyelid tissues.

The inflamed eyelid tissue develops swelling with increased vascular permeability and leakage of plasma. The volume of the swollen tissue was expanded by leaking plasma. Because the plasma is composed of 91% water and the reduced scattering coefficient of water is very low, the reduced scattering coefficient of the swollen tissue expanded by plasma decreases. As shown in Fig. 9(b), the reduced scattering coefficients of the MGD group are significantly lower than those of the control group at most wavelengths. This shows that inflammation-induced eyelid swelling can be quantitatively identified with a decrease in the scattering coefficient measured by the SFDI method. In the MGD group results, the reduced scattering coefficient of the MG region was significantly different from that of the non-MG region. This may be attributed to the increased lipid concentration, which can be caused by inflammatory MGD in the MG regions. As plasma is a low-scattering substance but lipids are strong scatterers, it is thought that the increase in lipid concentration alleviates the decrease in the reduced scattering coefficient of the MG-region rather than the non-MG-region in the MGD group. As shown in Fig. 9(b), the decrease rate of the average reduced scattering coefficient of the MGD group to the control group is approximately 16.8% in the MG region and lower than approximately 44.5% in the non-MG region. This needs to be confirmed by measuring the lipid concentration. However, it is challenging to measure the lipid concentration with the SFDI system using a light source in the 600–800-nm wavelength band. To quantitatively measure the lipid concentration, additional studies using a 900–1700-nm SWIR SFDI are required.

The optical properties and Hb concentrations measured in our experiments have sorts of inaccuracies for two reasons. The first reason is thickness issue. Since the thickness of the rat eyelids and MGs are about 2.7 mm and about 0.3 mm, respectively, our measured eyelids and MGs are not thick enough to fully approximate a semi-infinite medium condition. Also, the sample plate of a white PVC form sheet placed beneath the thin eyelid tissue can affect the measured values of optical properties and Hb concentrations. So, the measured optical properties and Hb concentration may have certain discrepancies in absolute values compared to the measurement in a thick medium condition. But, in case the thin medium on a white plate with a high reflectance, the monotonic increasement of optical properties according to the increasing chromophore concentration can be maintained. The second reason is the limited spatial resolution of an SFDI device. The width and length of a single MG are 0.3 mm and 1 mm, respectively. And the spacing distance between two adjacent MGs is approximately 0.1 mm. Since transport mean-free path in common biological tissues in the NIR spectral band is about 1 mm [30], the spatial resolution of an SFDI system is not high enough to separate accurately MGs from non-MG tissues. So, the optical properties and Hb concentration measured in the small size ROIs which we want to see can be affected by those in adjacent other tissue regions due to the limited spatial resolution. However, although the inaccuracies in absolute measured values and the incomplete MG ROI separations from other tissues exist in our experiment due to the reasons described above, when the eyelid tissue was equally approximated to the semi-infinite medium, the significant differences between MGD and control groups were observed in optical properties

Biomedical Optics EXPRESS

and Hb concentration. These results indicate that the relative changes in optical properties and Hb concentration caused by eyelid MGD can be detected through an SFDI even in thin and narrow tissues such as eyelids containing MGs. As a future work, an advanced SFDI technique for accurate absolute value measurement in thin and small size tissue medium like eyelids is expected.

In this study, we verified that an SFDI method can detect variations in the optical properties and Hb concentrations in *ex-vivo* SD-rat eyelid tissues with induced inflammatory MGD. To extend this study to *in-vivo* MG measurements, three major advancements are required. First, as SFDI is generally vulnerable to motion artifacts [21], motion artifacts from eye blinks or head shaking can degrade the quality of the SFDI results. So, animal anesthesia may be necessary to remove the motion artifacts. Moreover, to eliminate breathing motion artifacts under anesthesia, a fast SFDI method such as the single snapshot imaging (SSOP) reported by Ghijsen et al. could be a solution [22,23]. Second, as a considerable amount of HbO_2 exists in the blood vessels of live tissue, HbO_2 should be considered for the calculation of the chromophore concentration. Third, an SFDI device using the SWIR light source which has long wavelengths between 900 to 1700 nm is required to accurately measure the lipid concentration of MG.

5. Conclusions

In this study, we performed quantitative and noninvasive optical property and Hb concentration measurements of the eyelid tissues of SD rats using our implemented SFDI system to investigate a method to detect inflammatory MGD. To induce MGD, CFA was injected into the SD rats. After three weeks, the SD rats were diagnosed using two conventional methods to verify the MGD induction. The optical properties and Hb concentration for all *ex-vivo* MGs of SD rats were measured using the SFDI system. MG regions can be isolated from eyelid tissue images through image processing, such as adaptive local contrast enhancement and intensity contrast classification. Finally, we compared the Hb concentrations and optical properties of the MGD and control groups. In the comparison of Hb concentration results, the MGD group exhibited significantly higher values than the control group. Furthermore, the reduced scattering coefficients of the MGs at 730 and 850 nm were significantly different between the MGD and control groups. The absorption coefficients of the MGs were also significantly different. Therefore, we confirmed that the variations in optical properties and Hb concentration due to inflammatory MGD can be detected by the implemented SFDI system. The measurement of Hb concentration and optical properties using the SFDI method could be utilized in MGD diagnosis.

Funding. Ministry of Education (NRF-2017R1D1A1B03035027); Ministry of Science and ICT, South Korea (NRF-2018K1A4A3A02060572).

Acknowledgments. This research was supported by Basic Science Research Program through the National Research Foundation of Korea (NRF) funded by the Ministry of Education (NRF-2017R1D1A1B03035027) and Leading Foreign Research Institute Recruitment Program through the NRF funded by the Ministry of Science and ICT (MSIT) (NRF-2018K1A4A3A02060572). The authors thank Dr. Kyong Jin Cho's lab., Dankook University, Korea, for the assistance in animal experiments.

Disclosures. The authors declare no conflicts of interest.

Data availability. Data underlying the results presented in this paper are not publicly available at this time but may be obtained from the authors upon reasonable request.

References

1. J. M. Tiffany, "The lipid secretion of the meibomian glands," Adv. Lipid Res. **22**, 1–62 (1987).
2. E. Goto, Y. Monden, Y. Takano, A. Mori, S. Shimmura, J. Shimazaki, and K. Tsubota, "Treatment of non-inflamed obstructive meibomian gland dysfunction by an infrared warm compression device," Br. J. Ophthalmol. **86**(12), 1403–1407 (2002).
3. M. A. Lemp, C. Baudouin, J. Baum, M. Dogru, G. N. Foulks, S. Kinoshita, P. Laibson, J. McCulley, J. Murube, S. C. Pflugfelder, M. Rolando, and I. Toda, "The definition and classification of dry eye disease: report of the definition and classification subcommittee of the International Dry Eye WorkShop (2007)," Ocul. Surf. **5**(2), 75–92 (2007).

Biomedical Optics EXPRESS

4. A. J. Bron, L. Benjamin, and G. R. Snibson, "Meibomian gland disease: classification and grading of lid changes," Eye **5**(4), 395–411 (1991).
5. C. Celsus and L. Pasteur, "Natural resolution of inflammation," Periodontol. **63**, 149–164 (2013).
6. C. Baudouin, E. M. Messmer, P. Aragona, G. Geerling, Y. A. Akova, J. Benítez-Del-Castillo, K. G. Boboridis, J. Merayo-Lloves, M. Rolando, and M. Labetoulle, "Revisiting the vicious circle of dry eye disease: a focus on the pathophysiology of meibomian gland dysfunction," Br. J. Ophthalmol. **100**(3), 300–306 (2016).
7. A. Peral, J. Alonso, and J. A. Gomez-Pedrero, "Effect of illuminating wavelength on the contrast of meibography images," OSA Continuum **1**(3), 1041–1054 (2018).
8. K. Lekhanont, P. Jongkhajornpong, V. Sontichai, T. Anothaisintawee, and S. Nijvipakul, "Evaluating dry eye and meibomian gland dysfunction with meibography in patients with Stevens–Johnson Syndrome," Cornea **38**(12), 1–6 (2019).
9. R. Arita, K. Itoh, K. Inoue, and S. Amano, "Noncontact infrared meibography to document age-related changes of the meibomian glands in a normal population," Ophthalmology **115**(5), 911–915 (2008).
10. J. J. Nichols, D. A. Berntsen, G. L. Mitchell, and K. K. Nichols, "An assessment of grading scales for meibography images," Cornea **24**(4), 382–388 (2005).
11. C.K.S. Chew, C. Jansweijer, J.M. Tiffany, S. Dikstein, and A.J. Bron, "An instrument for quantifying meibomian lipid on the lid margin: the Meibometer," Curr. Eye Res. **12**(3), 247–254 (1993).
12. N. Yokoi, F. Mossa, J. M. Tiffany, and A. J. Bron, "Assessment of meibomian gland function in dry eye using meibometry," Arch. Ophthalmol. **117**(6), 723–729 (1999).
13. C. A. McCarty, A. K. Bansal, P. M. Livingston, Y. L. Stanislavsky, and H. R. Taylor, "The epidemiology of dry eye in Melbourne, Australia," Ophthalmology **105**(6), 1114–1119 (1998).
14. R. Toyos, W. McGill, and D. Briscoe, "Intense pulsed light treatment for dry eye disease due to meibomian gland dysfunction; a 3-year retrospective study," Photomed. Laser Surg. **33**(1), 41–46 (2015).
15. Y. Eom, K. E. Choi, S. Y. Kang, H. K. Lee, H. M. Kim, and J. S. Song, "Comparison of meibomian gland loss and expressed meibum grade between the upper and lower eyelids in patients with obstructive meibomian gland dysfunction," Cornea **33**(5), 448–452 (2014).
16. A. J. Lin, A. Ponticorvo, S. D. Konecky, H. Cui, T. B. Rice, B. Choi, A. J. Durkin, and B. J. Tromberg, "Visible spatial frequency domain imaging with a digital light microprojector," J. Biomed. Opt. **18**(9), 096007 (2013).
17. D. J. Cuccia, F. Bevilacqua, A. J. Durkin, F. R. Ayers, and B. J. Tromberg, "Quantitation and mapping of tissue optical properties using modulated imaging," J. Biomed. Opt. **14**(2), 024012 (2009).
18. T. A. Erickson, A. Mazhar, D. Cuccia, A. J. Durkin, and J. W. Tunnell, "Lookup-table method for imaging optical properties with structured illumination beyond the diffusion theory regime," J. Biomed. Opt. **15**(3), 036013 (2010).
19. J. R. Weber, D. J. Cuccia, A. J. Durkin, and B. J. Tromberg, "Noncontact imaging of absorption and scattering in layered tissue using spatially modulated structured light," J. Appl. Phys. **105**(10), 102028 (2009).
20. M. Torabzadeh, I. Park, R. A. Bartels, A. J. Durkin, and B. J. Tromberg, "Compressed single pixel imaging in the spatial frequency domain," J. Biomed. Opt. **22**(3), 030501 (2017).
21. A. Mazhar, S. Dell, D. J. Cuccia, S. Gioux, A. J. Durkin, J. V. Frangioni, and B. J. Tromberg, "Wavelength optimization for rapid chromophore mapping using spatial frequency domain imaging," J. Biomed. Opt. **15**(6), 061716 (2010).
22. M. Ghijsen, B. Choi, A. J. Durkin, S. Gioux, and B. J. Tromberg, "Real-time simultaneous single snapshot of optical properties and blood flow using coherent spatial frequency domain imaging (cSFDI)," Biomed. Opt. Express **7**(3), 870 (2016).
23. R. H. Wilson, C. Crouzet, M. Torabzadeh, and A. Bazrafkan, "High-speed spatial frequency domain imaging of rat cortex detects dynamic optical and physiological properties following cardiac arrest and resuscitation," Neurophotonics **4**(04), 1 (2017).
24. H. Miyake, T. Oda, O. Katsuta, M. Seno, and M. Nakamura, "A novel model of meibomian gland dysfunction induced with complete Freund's adjuvant in rabbits," Vision **1**(1), 10 (2017).
25. Y. Tang, H. Chang, C. Chiang, C. Lai, M. Hsu, H. Han, L. Chen, and D. P. Lin, "A murine model of acute allergic conjunctivitis induced by continuous exposure to particulate matter 2.5," Invest. Ophthalmol. Vis. Sci. **60**(6), 2118–2126 (2019).
26. M. A. A. Neil, R. Juskaitis, and T. Wilson, "Method of obtaining optical sectioning by using structured light in a conventional microscope," Opt. Lett. **22**(24), 1905–1907 (1997).
27. R. B. Saager, D. J. Cuccia, and A. J. Durkin, "Determination of optical properties of turbid media spanning visible and near-infrared regimes via spatially modulated quantitative spectroscopy," J. Biomed. Opt. **15**(1), 017012 (2010).
28. K. Zuiderveld, "Contrast limited adaptive histograph equalization," in *Graphic Gems IV* (Academic Press Professional, 1994), 474–485.
29. R. B. Saager, R. A. Rowland, M. L. Baldado, G. T. Kennedy, N. P. Bernal, A. Ponticorvo, R. J. Christy, and A. J. Durkin, "Impact of hemoglobin breakdown products in the spectral analysis of burn wounds using spatial frequency domain spectroscopy," J. Biomed. Opt. **24**(02), 1 (2019).
30. T. D. O'Sullivan, A. E. Cerussi, B. J. Tromberg, and D. J. Cuccia, "Diffuse optical imaging using spatially and temporally modulated light," J. Biomed. Opt. **17**(7), 071311 (2012).